Int J Thermophys
DOI 10.1007/s10765-013-1477-0

Measurement of Thermal Properties of Biosourced Building Materials

Thomas Pierre · Thibaut Colinart · Patrick Glouannec

Received: 18 June 2012 / Accepted: 17 June 2013

Abstract This paper presents both experimental and theoretical works concerning the evaluation of the thermal conductivity and thermal diffusivity of hemp concrete. Experimental measurements of thermal properties are performed using a hot-strip technique for temperatures ranging from −3 °C to 30 °C and relative humidities ranging from 0 % to 95 %, thus creating a large database for this material. These experimental thermal conductivities are then compared with the results from the Krischer theoretical predictive model. The comparison shows good agreement, and a predictive analytical relation between the hemp concrete thermal conductivity, temperature, and relative humidity is determined.

Keywords Hemp concrete · Moisture content · Predictive model · Temperature dependence · Thermal conductivity · Thermal diffusivity

List of Symbols

Variables

a	Thermal diffusivity ($m^2 \cdot s^{-1}$)
b	Hot-strip halfwidth (m)
c_p	Specific heat ($J \cdot kg^{-1} \cdot K^{-1}$)
mc_{hs}	Specific heat capacity ($J \cdot K^{-1}$)
p	Laplace parameter

T. Pierre (✉) · T. Colinart · P. Glouannec
Laboratoire d'Ingénierie des MATériaux de Bretagne (LIMATB)—EA4250,
Université de Bretagne-Sud, Université Européenne de Bretagne,
Rue de Saint Maudé, BP 92 116, 56 321 Lorient Cedex, France
e-mail: thomas.pierre@univ-ubs.fr

Published online: 19 July 2013

t	Time (s)
t_c	Critical time (s)
u_n	Transcendental solutions (m^{-1})
x, y, z	Cartesian coordinates
w	Water content ($kg \cdot kg^{-1}$)
w_0	GAB's model coefficient ($kg \cdot kg^{-1}$)
I	Current (A)
C	GAB's model coefficient
E	Thermal effusivity ($J \cdot m^{-2} \cdot K^{-1} \cdot s^{-1/2}$)
H	Sample height (m)
K	GAB's model coefficient
L	Sample halfwidth (m)
N	Norm
R_c	Contact resistance ($K \cdot W^{-1}$)
RH	Relative humidity (%)
S	Saturation
S_c	Contact surface area (m^2)
T	Temperature (°C or K)
U	Voltage (V)
X	Reduced sensitivity

Greek

α_n	Eigenvalue
β_i	Parameter
ε	Porosity
θ	Laplace space temperature (°C or K)
λ	Thermal conductivity ($W \cdot m^{-1} \cdot K^{-1}$)
ρ	Density ($kg \cdot m^{-3}$)
φ	Laplace space flux (W)
ψ	Eigenfunction
ϕ	Time space flux (W)

Exponents, subscripts

a	Dry air
c	Contact
eff	Effective
exp	Experimental
hs	Hot-strip
s	Solid
w	Moisture (liquid and vapor phases)
$\perp$	Orthogonal
//	Parallel

1 Introduction

In recent years, attention has been paid to reduce energy consumption in buildings. For example, improving efficiency, ventilation, and air conditioning systems (HVAC) is one of the challenges. One simple way consists in paying attention to building design and mainly to its envelope because it is the main barrier of protection from the outside conditions, such as cold in winter, heat in summer, humidity, rain, wind, and noise [1]. Because of growing environmental consciousness, biosourced building materials are increasingly used nowadays in building envelopes for their interesting attributes such as low weight, low thermal conductivity, environmentally friendly, easily industrialized, or easy on-site casting [2]. Hemp-based materials are one of them and present potentially large possibilities in building construction [3–6].

Hemp concrete is made from vegetal aggregates such as hemp shives (or hemp hurds) and a lime binder. With the appropriate proportion of hemp and binder, hemp concrete can cover different uses in a building [7]: roof insulation (minimal coating of hemp shives to attach them to each other), wall (good compromise between thermal and mechanical properties), and ground floor insulating slab (the higher proportion of lime, the greater mechanical properties). Similar to the classical concrete, three different processes are developed for setting up hemp concrete [7]: (i) molding of prefabricated blocks, (ii) mechanical mixing, and (iii) tamping and spraying. Whatever the process, mechanical or manual compaction could induce a preferential orientation of the hemp particles, as shown in Fig. 1a (top view) and Fig. 1b (X-ray tomography). Whatever the formulation or the setting process, previous research performed at the material scale pointed out that hemp concrete has a low bulk density ($300\,\mathrm{kg \cdot m^{-3}} < \rho < 600\,\mathrm{kg \cdot m^{-3}}$) [7] and a high porosity ($\varepsilon > 0.65$) [8,9]; therefore, hemp concrete presents low mechanical properties and could not be used for structural purposes until now [10,11]. On the other hand, previous studies indicate that the dry thermal conductivity at ambient temperature (λ) lies between $0.05\,\mathrm{W \cdot m^{-1} \cdot K^{-1}}$ and $0.15\,\mathrm{W \cdot m^{-1} \cdot K^{-1}}$ [9–11].

The knowledge of a single characteristic value may nevertheless not be sufficient to represent the thermal behavior of the material since it is well known that temperature [12] and moisture content due to hygroscopic behavior [8] influence thermal properties during climatic changes: a significant amount of pores is filled with water, for which the thermal conductivity is $0.600\,\mathrm{W \cdot m^{-1} \cdot K^{-1}}$, while that of air is $0.026\,\mathrm{W \cdot m^{-1} \cdot K^{-1}}$. The consequence of the presence of these three phases (solid matrix, air, and water)

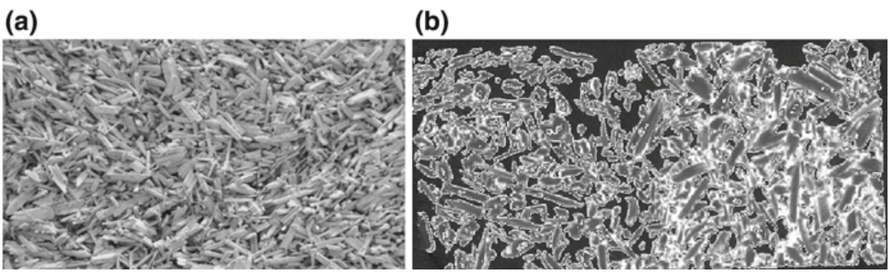

Fig. 1 (a) Focused and (b) tomographic views of a hemp concrete

and the competition of their effects among them will determine the effective thermal properties of the hemp concrete. For example, common exercises on heat, air, and moisture (HAM) transfer have demonstrated the importance of correct evaluation of heat and airflow balances and of the material properties on temperature and moisture calculations [13]. So, the motivation for determination of the effective thermal conductivity of such a porous material as a function of temperature and moisture content appears very significant.

In this work, an experimental procedure is developed to assess temperature and relative humidity (*RH*) dependence of hemp concrete's thermal properties. The effective thermal conductivity and thermal diffusivity of two hemp concrete samples are estimated by the inverse method and by using the hot-strip technique (Sect. 2). The measured values of thermal conductivity are then compared with the results from a predictive model, namely the Krischer model (Sect. 3).

2 Materials and Techniques

2.1 Experimental Facility

The thermal conductivity can be experimentally determined either by steady-state or transient methods [14]. A measurement method is selected based on the following criteria: the size of the representative elementary volume, temperature range, and thermal-conductivity range [15]. In our case, measurements are performed with a hot-strip [16]. This technique represents a fast and accurate method to measure thermal transport properties for a wide range of materials, even highly porous building materials [17], and can be used to measure the thermal conductivity from low ($0.005\,\mathrm{W \cdot m^{-1} \cdot K^{-1}}$) to high values (above $50\,\mathrm{W \cdot m^{-1} \cdot K^{-1}}$) over a wide temperature range [18].

As presented in Fig. 2, the hot-strip used in this work is a Kapton® heating element of (25.40 ± 0.01) mm in width ($2b$) and (50.80 ± 0.01) mm in length (Minco HK5164R78.4L12), with an electrical resistance R equal to 115 Ω. The hot-strip is coated with a very thin aluminum layer in order to homogenize the heat flux. The temperature is measured by a type K thermocouple. A flux step is experimentally applied to the hot-strip disposed between two identical $(100 \times 100 \times 30)\,\mathrm{mm}^3$ samples. The measurement consists in recording, every 0.5 s, the temperature T, the current I flowing through the hot-strip, and the voltage U. The flux, given by $\phi = UI/2$, can then be calculated. These measurements are then interpreted in terms of thermal properties using a theoretical model and an inverse method (see Sects. 2.2 and 2.3).

For evaluating the dependence of the thermal properties on the temperature and on the *RH*, a special device is developed (see Fig. 3). The samples are first placed in a desiccator where the *RH* is controlled by saturated salt solutions. Then, the desiccator is placed in a box where the temperature is controlled. At that point, the samples are equilibrated at one *RH* level for at least one week. After that, the temperature is lowered step-by-step from 30 °C to −3 °C and at least three measurements are performed in both constant *RH* and temperature (see Fig. 4). During all the experiments, the ambient temperature and *RH* are also recorded. Before and after each experiment at constant *RH*, the samples are weighted in order to get the dry-basis water content w.

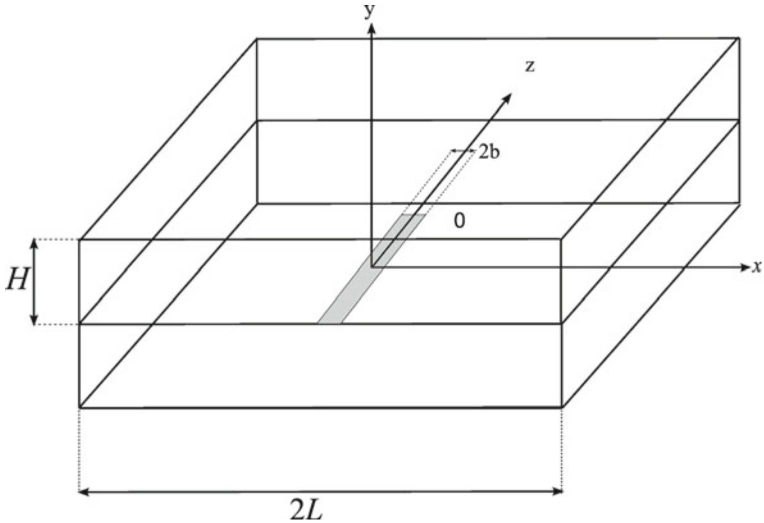

Fig. 2 Hot-strip disposition between the two samples

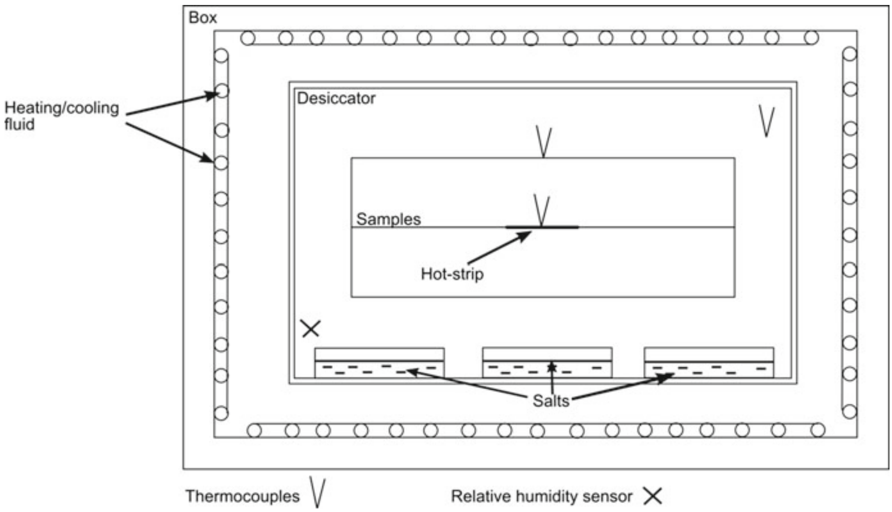

Fig. 3 Experimental apparatus for the hot-strip measurement under controlled temperature and relative humidity

2.2 Analytical Model

In this section, a theoretical model of the hot-strip experiment is developed (Fig. 2). Neglecting the mass transfers, the model is assumed to be purely conductive and two-dimensional (2D). The heat equation at $z = 0$ is

$$\frac{\partial^2 T\,(x, y, t)}{\partial x^2} + \frac{\partial^2 T\,(x, y, t)}{\partial y^2} = \frac{1}{a}\frac{\partial T\,(x, y, t)}{\partial x} \tag{1}$$

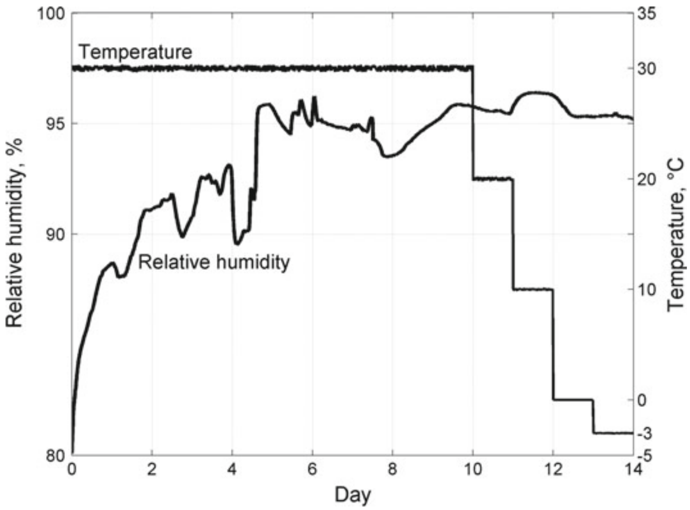

Fig. 4 Conditioning protocol in *RH* and in temperature of the samples. Example given for *RH* going up from 80 % to 95 % and for temperature going down from 35 °C to −3 °C

The time and boundary conditions are normalized as follows:

$$t = 0 \qquad T(x, y, 0) = 0 \tag{2}$$

$$x = 0 \qquad \frac{\partial T(0, y, t)}{\partial x} = 0 \tag{3}$$

$$x = L \qquad T(L, y, t) = 0 \text{ (semi-infinite assumption)} \tag{4}$$

$$y = H \qquad T(x, H, t) = 0 \text{ (semi-infinite assumption)} \tag{5}$$

$$y = 0 \text{ and } x \leq b \qquad \lambda S_{\mathrm{c}} \frac{\partial T(x, 0, t)}{\partial y} = \phi \tag{6}$$

$$x > b \qquad \frac{\partial T(x, 0, t)}{\partial y} = 0 \tag{7}$$

For both the temperature and flux, a double integral transform in space according to the x-direction (cosine) and time (Laplace) [19] leads to

$$\theta(\alpha_n, y, p) = \int_{t=0}^{\infty} \int_{x=0}^{L} T(x, y, t) \cos(\alpha_n x)\, \mathrm{e}^{-pt} \mathrm{d}x\mathrm{d}t \tag{8}$$

and allows one to get the following equation:

$$\frac{\mathrm{d}^2\theta(\alpha_n, y, p)}{\mathrm{d}y^2} = \left(\frac{p}{a} + \alpha_n^2\right) \theta(\alpha_n, y, p) \tag{9}$$

with $\alpha_n = (n + 1/2)\pi/L$ and p the Laplace parameter. The solution of Eq. 9 is

$$\theta(\alpha_n, y, p) = A \cosh(u_n y) + B \sinh(u_n y) \tag{10}$$

with $u_n^2 = p/a + \alpha_n^2$. The same double integral transform concerning the flux ϕ is also needed:

$$\varphi(\alpha_n, y, p) = \int_0^b \phi \cos(\alpha_n x)\, \mathrm{d}x = \phi \frac{\sin(\alpha_n b)}{\alpha_n} \tag{11}$$

Through the y-direction, the medium is multilayered and composed by the heating element, a contact resistance, and the sample. The quadrupole formalism and solutions of Eq. 10 are used to express the heat transfer [20] as follows:

$$\underbrace{\begin{bmatrix} \theta(\alpha_n, 0, p) \\ \varphi(\alpha_n, 0, p) \end{bmatrix}}_{y=0 \text{ temperature and flux}} = \underbrace{\begin{bmatrix} 1 & 0 \\ mc_{\mathrm{hs}} p & 1 \end{bmatrix}}_{\text{hot-strip}} \underbrace{\begin{bmatrix} 1 & R_{\mathrm{c}} \\ 0 & 1 \end{bmatrix}}_{\text{contact resistance}} \underbrace{\begin{bmatrix} A_m & B_m \\ C_m & D_m \end{bmatrix}}_{\text{sample}} \underbrace{\begin{bmatrix} \theta(\alpha_n, H, p) \\ \varphi(\alpha_n, H, p) \end{bmatrix}}_{y=H \text{ temperature and flux}} \tag{12}$$

with

$$A_m = D_m = \cosh(u_n H) \tag{13}$$

$$B_m = \frac{1}{\lambda S_{\mathrm{c}} u_n} \sinh(u_n H) \tag{14}$$

$$C_m = \lambda S_{\mathrm{c}} u_n \sinh(u_n H) \tag{15}$$

The solution is

$$\theta(\alpha_n, 0, p) = \frac{1 + S_{\mathrm{c}} R_{\mathrm{c}} \lambda u_n}{mc_{\mathrm{hs}} p (1 + S_{\mathrm{c}} R_{\mathrm{c}} \lambda u_n) + S_{\mathrm{c}} \lambda u_n} \frac{\phi}{p} \frac{\sin(\alpha_n b)}{\alpha_n} \tag{16}$$

From Eq. 16, a first inverse integral transform is made:

$$\overline{T}(0, 0, p) = \sum_{n=1}^{\infty} \frac{\psi(\alpha_n, 0)}{N(\alpha_n)} \theta(\alpha_n, 0, p) = \frac{2}{L} \sum_{n=1}^{\infty} \theta(\alpha_n, 0, p) \tag{17}$$

where $\psi(\alpha_n, 0) = \cos(\alpha_n y)$ is the eigenfunction and $N(\alpha_n) = L/2$ is the norm of $\theta(\alpha_n, 0, p)$ [20]. Equation 17 determines the temperature at the center of the hot-strip. Finally, $T(0, 0, t)$ is obtained thanks to a numerical inverse Laplace transform.

2.3 Inverse Problem: Sensitivity Analysis and Parameter Estimation

The theoretical model has first been used to calculate the sensitivity of the temperature $T(0, 0, t)$ of the hot-strip to the thermal conductivity λ, the thermal effusivity $E = \lambda a^{-1/2}$, the contact resistance R_{c}, and the hot-strip specific heat capacity mc_{hs}. The aim of this study is to verify that these parameters have no correlated influence on $T(0, 0, t)$ and a sufficient sensitivity level so that they could be properly and precisely estimated.

The reduced sensitivity X_{β_i} of the temperature to the parameters β_i versus time is defined as

$$X_{\beta_i} = \beta_i \frac{\partial T}{\partial \beta_i} \tag{18}$$

Calculations have been made for a 25.4 mm wide hot-strip on hemp concrete with the following properties: $\lambda = 0.100\,\mathrm{W \cdot m^{-1} \cdot K^{-1}}$, $a = 2.5 \times 10^{-7}\,\mathrm{m^2 \cdot s^{-1}}$($E = 200\,\mathrm{J \cdot m^{-2} \cdot K^{-1} \cdot s^{-1/2}}$), $mc_{\mathrm{hs}} = 0.4\,\mathrm{J \cdot K^{-1}}$, and $R_{\mathrm{c}} = 5\,\mathrm{K \cdot W^{-1}}$. Figure 5 presents the evolutions of the temperature's reduced sensitivities to the estimated parameters.

Results show that:

- The reduced sensitivities of the temperature to the parameters behave differently from one another.
- The contact resistance and the specific heat can be estimated in the short time, e.g., $t < 40$ s. Then, they become less sensitive, the amplitude of $X_{mc_{\mathrm{hs}}}$ being greater than the amplitude of $X_{R_{\mathrm{c}}}$.
- X_E does not seem to be correlated to X_λ.
- The thermal conductivity λ can be estimated for great time ($t > 100$ s) and estimation of the thermal effusivity E is effective between 0 and 100 s.

We can infer from those results that estimation of the parameters λ, a, R_{c}, and mc_{hs} is theoretically possible. The semi-infinite assumption (Eqs. 4 and 5) has to be experimentally validated. For this, Fig. 6 presents the experimental temperature variation $T_{\mathrm{exp}}(0, 0, t)$ at the center of the hot-strip and $T_{\mathrm{exp}}(0, H, t)$ at the opposite surface of the sample. We observe that $T_{\mathrm{exp}}(0, H, t)$ remains constant until $t_c = 200$ s; thus, the estimation can be made between 0 and 180 s.

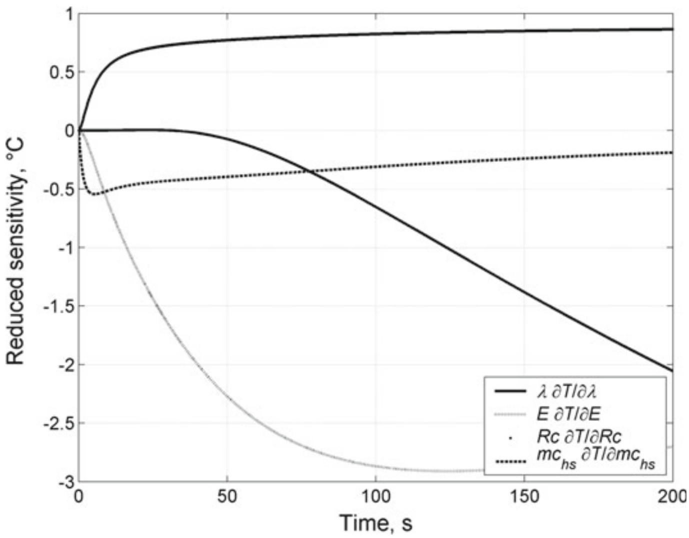

Fig. 5 Reduced sensitivity of T(0,0,t) to the thermal conductivity λ, the thermal effusivity E, the contact resistance R_{c}, and the specific capacity mc_{hs}

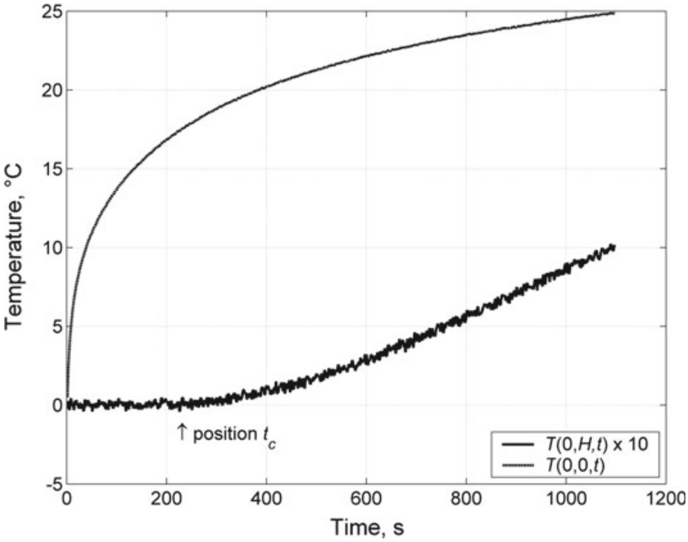

Fig. 6 Transient evolution of temperature at the center of the strip $T_{\text{exp}}(0, 0, t)$ and at the opposite surface of the sample $T_{\text{exp}}(0, H, t)$ and identification of the critical time t_c ($T_{\text{exp}}(0, H, t_c) > 0\,°\text{C}$)

The estimation is done by minimizing the quadratic error between the measured temperature $T_{\text{exp}}(0, 0, t)$ and $T(0, 0, t)$ with the least-squares coupled with a Levenberg–Marquardt algorithm. Figure 7a, b shows $T_{\text{exp}}(0, 0, t)$ and $T(0, 0, t)$, the experimental and theoretical temperatures calculated with the estimated parameters and also the residues $T(0, 0, t) - T_{\text{exp}}(0, 0, t)$ for two measurements at $RH = 0$ and 95 % and at constant temperature $T = 20\,°\text{C}$. The presence of water leads to a greater thermal conductivity and a lower temperature increase due to better heat transfer. The residue difference is less than 5 % between both estimations at $RH = 0$ and 95 %, which allows us to verify *a posteriori* that the mass transfer has minor influence on the heat transfer.

2.4 Results

This experimental procedure is applied to two hemp concrete samples since hemp concrete is anisotropic. In sample 1, hemp particles are oriented in the y-direction (see Fig. 8a), and in sample 2 they are oriented in the x-direction (see Fig. 8b). Both the samples are issued from the same hemp concrete, manufactured by projection with a wall formulation [7]. Tables 1 and 2 show the estimated parameters λ, a, R_c, and mc_{hs} for every temperature and every relative humidity for samples 1 and 2. Let us consider first the specific heat capacity mc_{hs}. It presents almost no dispersion and shows a global estimated value of $(0.45 \pm 0.05)\ \text{J} \cdot \text{K}^{-1}$ (about 8 %) for both samples. Since the hot-strip is the same for all experiments, a constant value of mc_{hs} confirms the estimation accuracy. The contact resistance R_c is constant for one *RH* regardless of the temperature, but it changes from one *RH* to the other. The experimental setup is, indeed, removed for changing the saturated salt solutions, and the compression of

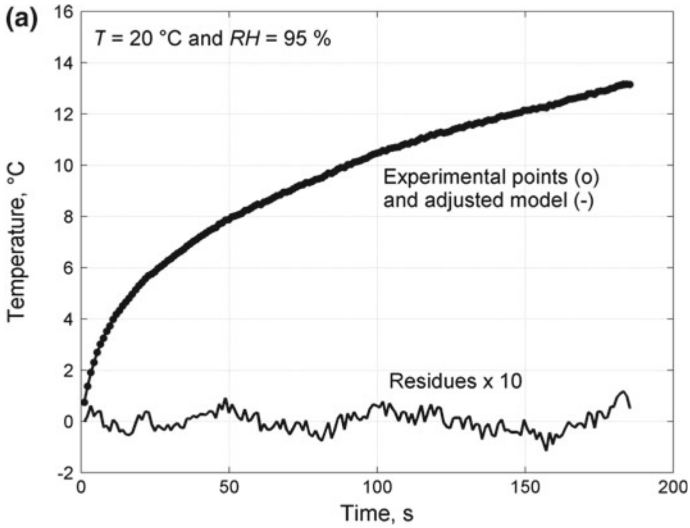

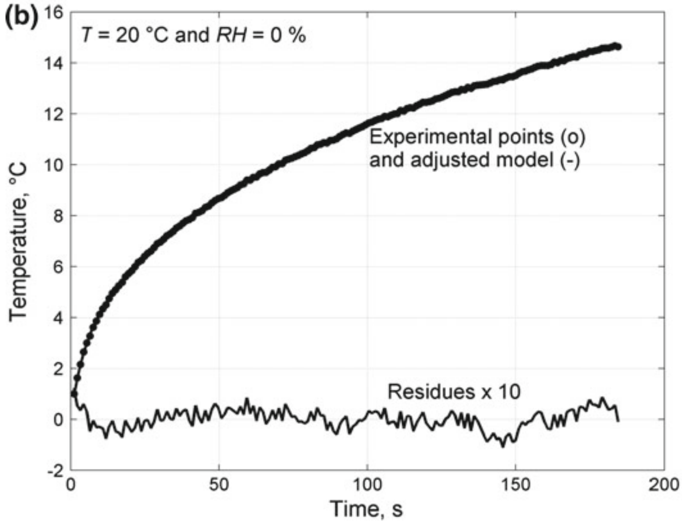

Fig. 7 Adjustment of the estimated temperature (−) on the experimental points and residues (×10) versus time for $T = 20\,°\mathrm{C}$ and two relative humidities: (a) *RH* = 0 and (b) *RH* = 95 %

the samples around the hot-strip is not controlled; nevertheless, this point does not disturb the estimation.

Focusing on the thermal diffusivity a, this parameter seems to increase with T and *RH* despite some outliers. Regardless, it shows values between $2.13 \times 10^{-7}\ \mathrm{m^2 \cdot s^{-1}}$ and $3.09 \times 10^{-7}\ \mathrm{m^2 \cdot s^{-1}}$. Tables 1 and 2 and Fig. 9 present the calculation of $\rho c_p = \lambda / a$ for the samples at $T = 20\,°\mathrm{C}$ functions of the water content w. We observe that the volumetric heat capacity ρc_p varies linearly with w. An additive model such as Eq. 19 can be compared to the experimental results [21].

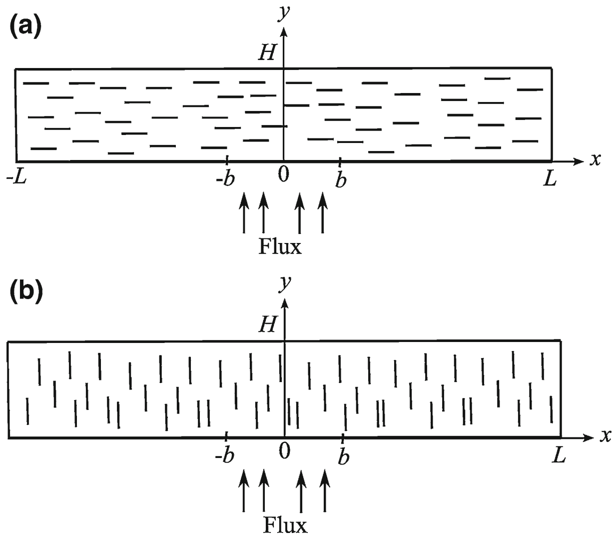

Fig. 8 Comparison for each sample of the vegetal particles orientation: according to (a) the y-direction and to (b) the x-direction

$$\rho c_{p,\mathrm{eff}} = \rho_{\mathrm{dry}} \left(c_{p,\mathrm{dry}} + w c_{p,\mathrm{w}} \right) \tag{19}$$

$\rho_{\mathrm{dry}} c_{p,\mathrm{dry}}$ is the volumetric specific heat of the dry hemp concrete ($\rho_{\mathrm{dry}} = \rho_{\mathrm{eff}}$ for $w = 0$ from Table 3) and $c_{p,\mathrm{w}}$ is the water specific heat. Experimental results are in good agreement with the model proposed by Eq. 19. The other experimental points cannot be plotted since the water content has only been measured for $T = 20\,°\mathrm{C}$. The order of magnitude of ρc_p is the same as that obtained experimentally from a micro-calorimetric measurement done in the laboratory.

Figure 10 presents the thermal conductivity variation with temperature and *RH* for both samples. As expected, the dry thermal conductivity λ clearly increases with T and ranges between $0.092\,\mathrm{W \cdot m^{-1} \cdot K^{-1}}$ and $0.100\,\mathrm{W \cdot m^{-1} \cdot K^{-1}}$ for sample 1 and between $0.069\,\mathrm{W \cdot m^{-1} \cdot K^{-1}}$ and $0.082\,\mathrm{W \cdot m^{-1} \cdot K^{-1}}$ for sample 2. As the relative humidity increases, the water content of both the samples increases (see Table 3 and Fig. 11), as well as the thermal conductivity λ. It confirms the role of water in heat conduction. Pavlík et *al.* [15] obtained similar trends on the thermal conductivity of a lime-based composite. Their thermal conductivity values for water-saturated samples are approximately three times higher than that for dry materials while only 1.5 times higher in the case of hemp concrete. It is interesting to note that the thermal conductivity is almost identical for -3 °C and 95 % *RH* (winter conditions) and for 30 °C and 66 % *RH* (summer conditions).

Finally, we observe that the dry thermal conductivity of sample 1 is higher than that of sample 2. As previously mentioned, the hemp shives are oriented in the y-direction for sample 1 and in the x-direction for sample 2 (assimilated in a series arrangement). It is well known that in the series arrangement the poorest conductor of its component layer dominates the overall heat conduction, while in the case of a

Table 1 Estimated parameters for sample 1 functions of *RH* and temperature

Setting temperature for $t = 0\,\mathrm{s}$ (°C)	Relative humidity (%)	0	42	66	80	95
−3	$\lambda (\mathrm{W \cdot m^{-1} \cdot K^{-1}})$	0.092	0.098	0.101	0.103	0.111
	$a\ (10^{-7}\,\mathrm{m^2 \cdot s^{-1}})$	2.46	2.48	2.53	3.02	2.73
	$R_c\ (\mathrm{K \cdot W^{-1}})$	7.93	16.65	9.07	13.81	4.68
	$mc_{hs}\ (\mathrm{J \cdot K^{-1}})$	0.42	0.43	0.40	0.30	0.58
0	λ	0.094	0.098	0.102	0.105	0.113
	a	2.81	2.66	2.74	2.81	3.29
	R_c	7.58	15.17	9.54	13.17	4.59
	mc_{hs}	0.43	0.41	0.45	0.42	0.45
10	λ	0.095	0.100	0.104	0.107	0.115
	a	2.53	2.64	2.42	2.90	3.03
	R_c	7.80	15.28	9.29	13.40	4.58
	mc_{hs}	0.44	0.45	0.46	0.40	0.53
20	λ	0.097	0.100	0.106	0.108	0.118
	a	2.79	2.74	2.74	2.65	2.54
	$\rho c_p\ (\mathrm{J \cdot m^{-3} \cdot K^{-1}})$	3.47	3.64	3.86	4.08	4.65
	R_c	7.47	15.15	8.64	13.48	4.17
	mc_{hs}	0.43	0.43	0.44	0.43	0.48
30	λ	0.100	0.103	0.109	0.112	0.122
	a	2.51	2.50	2.41	2.45	2.43
	R_c	7.78	14.32	8.97	13.27	4.75
	mc_{hs}	0.46	0.43	0.45	0.42	0.49
$\overline{R_c}\ (\mathrm{K \cdot W^{-1}})$		7.71 ± 0.18	15.31 ± 0.84	9.10 ± 0.34	13.43 ± 0.25	4.55 ± 0.23
$\overline{mc_{hs}}\ (\mathrm{J \cdot K^{-1}})$		0.44 ± 0.05				

Table 2 Estimated parameters for sample 2 functions of *RH* and temperature

Setting temperature for $t = 0\,\mathrm{s}$ (°C)	Relative humidity (%)	0	40	70	80	95
−3	$\lambda (\mathrm{W \cdot m^{-1} \cdot K^{-1}})$	0.069	0.073	0.074	0.080	0.092
	$a\,(10^{-7}\,\mathrm{m^2 \cdot s^{-1}})$	3.09	2.62	2.34	2.43	2.57
	$R_c\,(\mathrm{K \cdot W^{-1}})$	5.47	8.23	16.00	7.72	7.66
	$mc_{hs}\,(\mathrm{J \cdot K^{-1}})$	0.44	0.44	0.40	0.45	0.48
0	λ	0.073	0.078	0.079	0.082	0.093
	a	2.61	2.47	2.43	2.39	2.31
	R_c	5.32	8.47	16.01	7.29	7.75
	mc_{hs}	0.40	0.48	0.43	0.55	0.50
10	λ	0.073	0.079	0.081	0.085	0.097
	a	2.31	2.46	2.13	2.23	2.78
	R_c	5.44	8.79	16.25	7.80	7.30
	mc_{hs}	0.43	0.47	0.41	0.46	0.46
20	λ	0.079	0.079	0.090	0.093	0.101
	a	3.01	2.54	2.78	2.48	2.58
	$\rho c_p\,(\mathrm{J \cdot m^{-3} \cdot K^{-1}})$	2.62	3.11	3.23	3.75	3.91
	R_c	5.46	8.54	15.45	7.46	7.59
	mc_{hs}	0.44	0.50	0.40	0.45	0.48
30	λ	0.082	0.085	0.091	0.094	0.103
	a	2.61	2.59	2.22	2.33	2.51
	R_c	5.82	8.19	16.75	7.56	7.10
	mc_{hs}	0.47	0.46	0.49	0.45	0.49
$\overline{R_c}\,(\mathrm{K \cdot W^{-1}})$		5.50 ± 0.19	8.44 ± 0.24	16.09 ± 0.47	7.57 ± 0.20	7.48 ± 0.27
$\overline{mc_{hs}}\,(\mathrm{J \cdot K^{-1}})$		0.46 ± 0.04				

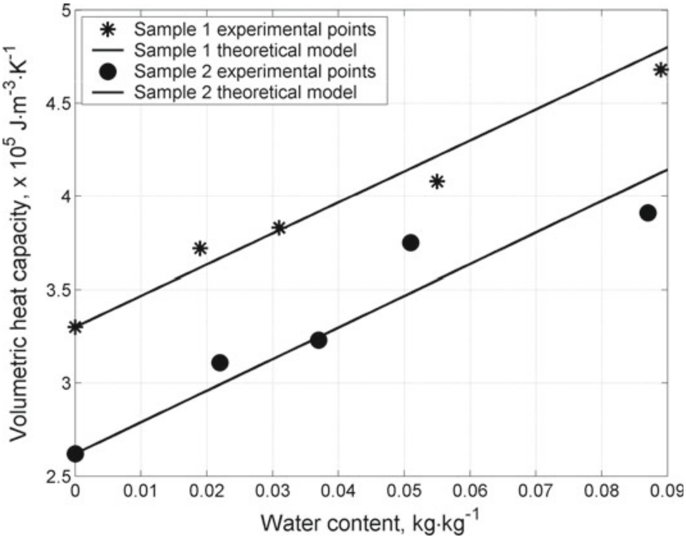

Fig. 9 Evolution of the volumetric heat capacity ρc_p of the samples versus the water content w for $T = 20\,°\mathrm{C}$

Table 3 Mass m, water content w, and effective density ρ_{eff} as function of the *RH* at $T = 20\,°\mathrm{C}$

Sample 1				Sample 2			
RH (%)	m (g)	w ($\mathrm{kg \cdot kg^{-1}}$)	ρ_{eff} ($\mathrm{kg \cdot m^{-3}}$)	RH (%)	m (g)	w ($\mathrm{kg \cdot kg^{-1}}$)	ρ_{eff} ($\mathrm{kg \cdot m^{-3}}$)
0	239.2	0.000	398.7	0	243.0	0.000	405.0
28	243.3	0.017	405.5	30	247.4	0.018	412.3
42	243.8	0.019	406.4	40	248.3	0.022	413.8
50	245.3	0.026	408.7	50	249.7	0.028	416.2
66	246.6	0.031	411.0	70	252.1	0.037	420.2
80	252.3	0.055	420.5	85	255.4	0.051	425.7
85	253.1	0.058	421.9	95	264.2	0.087	445.3
95	260.4	0.089	434.0				

parallel arrangement, the best conductor dominates the overall heat conduction. This point is respected for hemp concrete.

3 Predictive Model

Since the experimental measurement of thermal properties as a function of temperature and *RH* is very time consuming, development and application of predictive models are the most convenient method. In the literature, many works present the prediction of the effective thermal conductivity of porous media as a function of the phase (solid, liquid, gaseous), the porosity, the orientation, and the shape of the pores [22,23] or

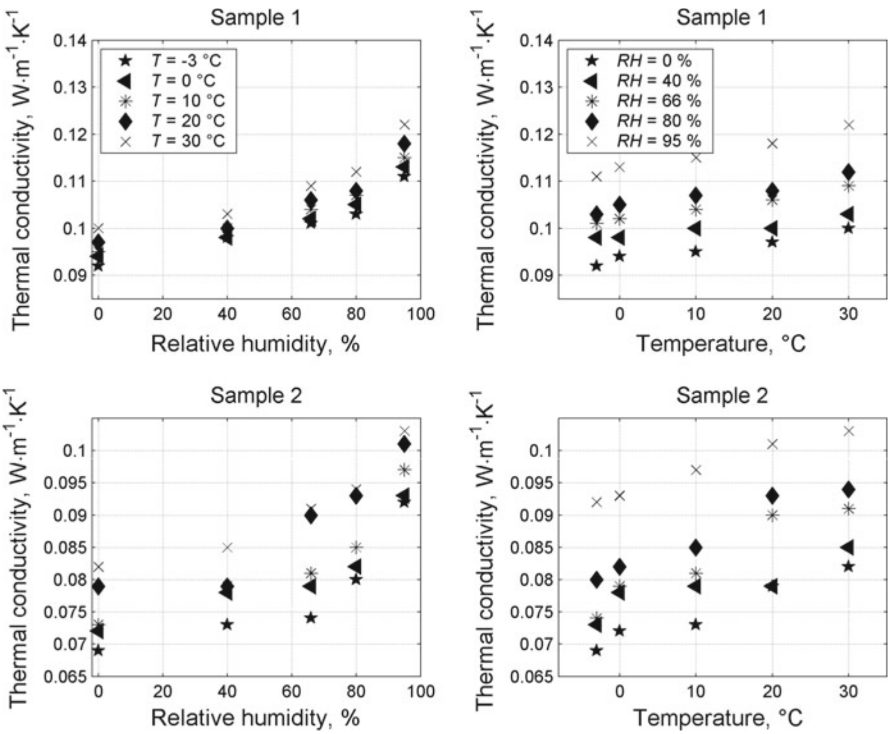

Fig. 10 Thermal conductivities as function of temperature and *RH* for both samples of hemp concrete

even the water content [24,25]. A review of models for the effective properties of multiphase materials can be found elsewhere [26].

Whatever the model, the effective thermal conductivity of a mixture should be chosen between two extreme values and given by the thermal conductivities and volumetric fractions of its constituents. The upper bound is reached in a system consisting of plane-parallel layers disposed alongside the heat flux vector. The lower bound is reached in a similar system but with the layers perpendicular to the heat flux. These bounds are usually called Wiener's bounds. In order to make these models more flexible or more generic, an extra parameter is sometimes introduced. For example, Krischer [27] proposed a weighted harmonic mean of the series and parallel models (see Fig. 12):

$$\lambda_{\text{eff}} = \frac{1}{\frac{1-n}{\lambda_{//}} + \frac{n}{\lambda_{\perp}}} \tag{20}$$

where the weighting parameter n ranges between 0 and 1. It is a common practice that n is the volume fraction of the medium disposed orthogonally to the heat flux direction. This model is very common because of its simplicity.

In our case, hemp concrete can be considered as a porous material composed of a solid phase (hemp and lime) and pores that can be filled with dry air or with moisture

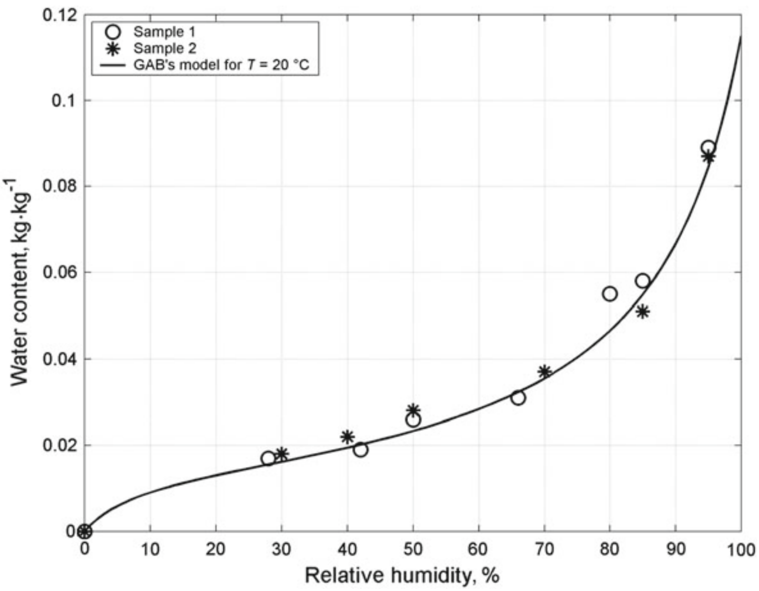

Fig. 11 Isothermal absorption curves for samples 1 and 2 and Guggenheim–Anderson–de Boer's (GAB) model fitting for $T = 20\,°\mathrm{C}$

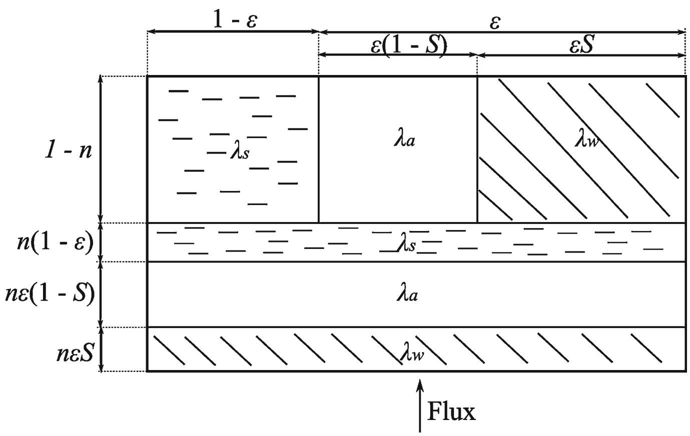

Fig. 12 Schematic description of the three-phase composite model by Krischer [27]

(vapor or liquid phase). The air volumetric fraction in a dry porous material is given by the total porosity ε $(0 \leq \varepsilon \leq 1)$. In the case of penetration of liquid water, the filled part of the porous space is given by the water saturation $S = \frac{\rho_{\mathrm{eff}}}{\rho_{\mathrm{w}}} \frac{w}{\varepsilon} (0 \leq S \leq 1)$. For this three-phase material, parallel ($\lambda_{//}$) and serial ($\lambda_{\perp}$) thermal conductivities are given by

$$\lambda_{//} = (1 - \varepsilon)\,\lambda_{\mathrm{s}} + \varepsilon\,(1 - S)\,\lambda_{\mathrm{a}} + \varepsilon S \lambda_{\mathrm{w}} \tag{21}$$

Table 4 Regression of temperature dependence from thermal conductivity (λ) and density (ρ) of air, water, and solid phase

Phase	$\lambda(T) = \sum_i p_i T^i$		$\rho(T) = \sum_i q_i T^i$	
	Order i	p_i	Order i	q_i
Air	2	$p_0 = 0.024452$	2	$q_0 = 1.296$
		$p_1 = 7.3245 \times 10^{-5}$		$q_1 = -0.0047964$
		$p_2 = -1.8674 \times 10^{-8}$		$q_2 = 1.21 \times 10^{-5}$
Water	2	$p_0 = 0.55692$	2	$q_0 = 1003.3$
		$p_1 = 0.0022603$		$q_1 = -0.15005$
		$p_2 = -1.109 \times 10^{-5}$		$q_2 = -0.0026716$
Solid phase	2	$p_0 = 0.3231$		
		$p_1 = 0.0018014$		
		$p_2 = -2.3562 \times 10^{-5}$		

The temperature range is (−3 °C to 30 °C)

$$\lambda_{\perp} = \frac{1}{\frac{1-\varepsilon}{\lambda_s} + \varepsilon\left(\frac{1-S}{\lambda_a} + \frac{S}{\lambda_w}\right)} \tag{22}$$

where λ_s, λ_w, and λ_a are the thermal conductivity of the solid phase, the moisture, and the dry air, respectively. The thermal conductivities of air and water are well known [12], and Table 4 gives their variations, $\lambda_a(T)$ and $\lambda_w(T)$, with temperature under polynomial forms in the working temperature range. Unlike the preceding values, the thermal conductivity λ_s of the solid phase is unknown (even if the order of magnitude of hemp shives and lime thermal conductivities are known).

The development of a predictive model is performed in two steps. First, the predictive model is fitted to the thermal conductivity of the dry material, for which only the solid and dry air phases are considered ($S = 0$). The unknown parameter λ_s, ε, and n are estimated using the least-squares with a Levenberg–Marquardt algorithm by minimizing the quadratic error between the experimental conductivities λ and λ_{eff} (from Eq. 20). Results are presented in Table 5 where a polynomial form for $\lambda_s(T)$ is deduced (Table 4). Regardless of the temperature, the structural parameters n and ε are constant. Specifically, the mean porosity of both samples is equal to 80.5 %, which is consistent with the 77 % measured by Collet [8]. As for the thermal conductivity of the solid phase λ_s, it is a function of the temperature and we note that the estimated values are similar for both the samples. The order of magnitude is also suitable since the values are contained between the thermal conductivity of lime ($5.5\,\text{W}\cdot\text{m}^{-1}\cdot\text{K}^{-1}$ [28]) and of cellulosic material ($0.050\,\text{W}\cdot\text{m}^{-1}\cdot\text{K}^{-1}$ [29]).

The second step in the procedure is the prediction of the thermal conductivity of the whole material, where the mixing is performed for the solid matrix, air, and water. For this problem, λ_s, n, and ε are considered as known (Table 3). Figures 13 and 14 present the predicted conductivities of both the hemp concrete samples as a function of the moisture content w and the experimental points. The estimation of the errors

Table 5 Results of Krischer's model estimations

Samples	T (°C)	−3	0	10	20	30
1	λ ($W \cdot m^{-1} \cdot K^{-1}$)	0.341	0.349	0.351	0.358	0.369
	ε	0.78				
	n	0.01				
2	λ ($W \cdot m^{-1} \cdot K^{-1}$)	0.293	0.310	0.313	0.345	0.360
	ε	0.83				
	n	0.01				

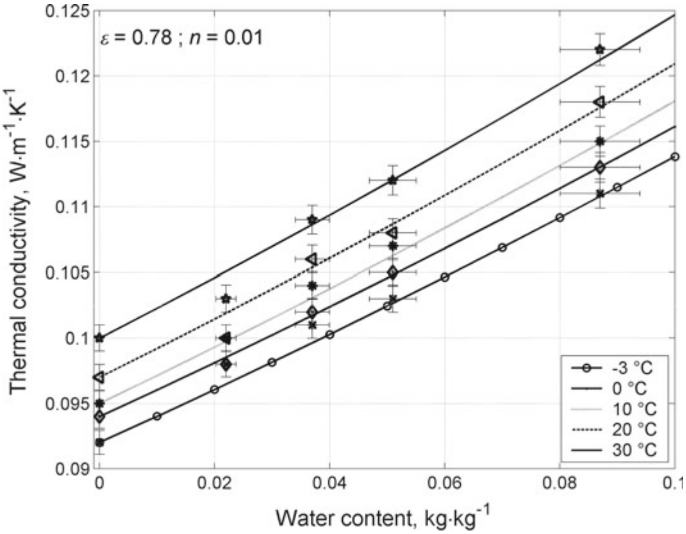

Fig. 13 Krischer's model adjustment on experimental thermal conductivities versus water content for sample 1

due to the water content and temperature measurements are also presented in Figs. 13 and 14. Thermal conductivity calculations have been carried out for a water content supposed to be constant between −3 °C and 30 °C (Table 3), since the experimental apparatus does not allow the measuring of the mass evolution during measurements. However, a 0.6 % mass variation has been observed before and after experiments, which leads to a water content variation of 8 % (horizontal error bar in Figs. 13 and 14). In parallel, the error on the thermal conductivity can be approached as the sum of the errors on the temperature measurement $T_{\text{exp}}(0, 0, t) - T_{\text{exp}}(0, 0, 0)$ (statistic error due to experimental noise of about 0.05 °C), on the hot-strip dimensions (systematic error of 0.1 %), and on the flux (systematic and statistical errors of 0.5 %). As a consequence, the error is estimated at 3 % on the thermal conductivity (vertical error bar in Figs. 13 and 14).

The comparison shows good agreement between predicted and experimental values and offers an interesting outlook. Indeed, the temperature and *RH* dependence of

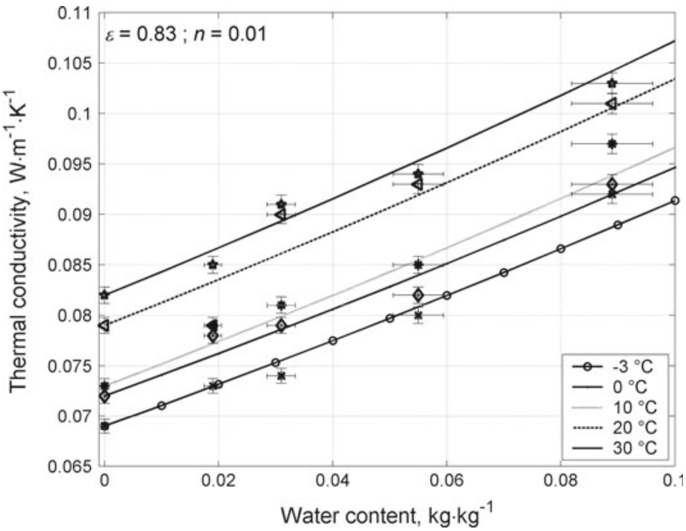

Fig. 14 Krischer's model adjustment on experimental thermal conductivities versus water content for sample 2

building materials may be evaluated by measuring the temperature dependence of dry materials and the isotherm sorption.

Finally, the thermal conductivity of hemp concrete can be expressed as a function of the temperature and the *RH* by

$$\lambda_{\mathrm{eff}}\left(T, w\right) = \left\{ \frac{1-n}{(1-\varepsilon)\lambda_{\mathrm{s}}(T)+\varepsilon\left[1-\frac{\rho_{\mathrm{dry}}(1+w)}{\rho_{\mathrm{w}}(T)}\frac{w}{\varepsilon}\right]\lambda_{\mathrm{a}}(T)+\frac{\rho_{\mathrm{dry}}(1+w)}{\rho_{\mathrm{w}}(T)}w\lambda_{\mathrm{w}}(T)} + \frac{n}{\frac{(1-\varepsilon)}{\lambda_{\mathrm{s}}(T)}+\frac{\varepsilon\left[1-\frac{\rho_{\mathrm{dry}}(1+w)}{\rho_{\mathrm{w}}(T)}\frac{w}{\varepsilon}\right]}{\lambda_{\mathrm{a}}(T)}+\frac{\frac{\rho_{\mathrm{dry}}(1+w)}{\rho_{\mathrm{w}}(T)}w}{\lambda_{\mathrm{w}}(T)}} \right\}^{-1} \tag{23}$$

The moisture content w can be expressed over the entire relative humidity *RH* range by fitting the GAB model [30] to the experimental data:

$$\frac{w}{w_0} = \frac{C\ K\ RH}{(1-K\ RH)\,(1-K\ RH - C\ K\ RH)} \tag{24}$$

where $w_0 = 0.0143\,\mathrm{kg}\cdot\mathrm{kg}^{-1}$, $C = 14.164$, and $K = 0.877$. These parameters have been estimated by least-squares by minimizing the quadratic error between the experimental water content (Table 3) and w from Eq. 24. Equations 23 and 24 may be helpful for investigating the heat and moisture transfer through a hemp concrete wall.

4 Conclusions

Application of bio-sourced materials (like hemp concrete) in building construction may be an interesting solution in order to improve sustainability and building energy efficiency. However, since it is a relatively new material, more knowledge is required. This study dealt with the characterization of the thermal properties of hemp concrete using the hot-strip technique. The thermal conductivity and the thermal diffusivity are estimated by inverse methods from temperature and heat flux measurements and by using a complete transient 2D analytical model. To investigate the influence of the temperature T and RH, a special experimental device was developed. Results indicate that the thermal conductivity increases when T increases from $-3\,^{\circ}\mathrm{C}$ to $30\,^{\circ}\mathrm{C}$ and/or RH increases from 0 to 95 %. Simultaneously, theoretical investigations are performed and it was shown that the predictive model of Krisher could successfully estimate the temperature and moisture dependence of the thermal conductivity of hemp concrete, thus providing a useful relation for HAM simulation.

Acknowledgment The authors would like to thank the European Union for the equipment co-financing through the European Regional Development Fund.

References

1. C. Maalouf, A.D. Le Tran, M. Lachi, E. Wurtz, T.H. Mai, Int. J. Math. Models Methods Appl. Sci. **5**, 33 (2011)
2. S. Hallyday, *Sustainable Construction* (Elsevier, Burlington, MA, 2008)
3. T. Woolley, H. Thompson, T. McGrogan, M. Alexander, *Proceedings of Sustainable Building Conference* (Stellenbosch, South Africa, 2004)
4. R. Bevan, T. Woolley, *Hemp Lime Construction: A Guide to Building with Hemp Lime Composites* (HIS BRE Press, Bracknell, 2008)
5. French Association "Construire en Chanvre," http://www.construction-chanvre.asso.fr. Accessed 12 June 2012
6. Final Report on the Construction of the Hemp Houses at Haverhill, Suffolk, Client Report Number 209–717, Rev. 1 (Building Research Establishment, 2002)
7. T. Colinart, P. Glouannec, P. Chauvelon, Constr. Build. Mater. **30**, 372 (2012)
8. F. Collet, M. Bart, L. Serres, J. Miriel, Constr. Build. Mater. **22**, 1271 (2008)
9. A. Evrard, Ph.D. Thesis, Universite Catholique de Louvain, 2008
10. T.T. Nguyen, V. Picandet, P. Carré, T. Lecompte, S. Amziane, C. Baley, Eur. J. Environ. Civil Eng. **14**, 545 (2010)
11. C. Magniont, G. Escadeillas, M. Coutand, C. Oms-Multon, Eur. J. Environ. Civil Eng. **16**, s17 (2012)
12. F.P. Incropera, D.P. DeWitt, *Fundamentals of Heat and Mass Transfer* (Wiley, New York, 2002)
13. M. Woloszyn, C. Rode, Build. Simul. **1**, 5 (2008)
14. E. Latif, R. Rhydwen, M. Pruteanu, C. Wijeyesekera, S. Tucker, M.A. Ciupala, D. Newport, Thermal Conductivity of Building Materials: An Overview of its Determination. Presented at Advances in Computing and Technology: 6th Annual Conference, University of East London, London, 2011
15. Z. Pavlík, E. Vejmelková, L. Fiala, R. Černý, Int. J. Thermophys. **30**, 1999 (2009)
16. Y. Jannot, P. Meukam, Meas. Sci. Technol. **15**, 1932 (2004)
17. A. Bouguerra, A. Aït-Mokhtar, O. Amiri, M.B. Diop, Int. Commun. Heat Mass Transf. **28**, 1065 (2001)
18. Y. He, Thermochim. Acta **436**, 122 (2005)
19. N. Ozisik, *Heat Conduction* (Wiley, New York, 2000)
20. D. Maillet, S. André, J.-C. Batsale, A. Degiovanni, C. Moyne, *Thermal Quadrupoles* (Wiley, Chichester, 2000)
21. H. Bal, Y. Jannot, N. Quenette, A. Chenu, S. Gaye, Constr. Build. Mater. **31**, 144 (2012)
22. J.C. Maxwell, *A Treatise on Electricity and Magnetism*, 3rd edn. (Dover Publication, New York, 1954)
23. R.L. Hamilton, O.K. Crosser, Ind. Eng. Chem. **1**, 187 (1969)
24. D.A. de Vries, N.H. Afgan, *Heat and Mass Transfer in the Biosphere* (Wiley, New York, 1972)
25. W.M. Rohsenow, J.P. Hartnett, Y.I. Cho, *Handbook of Heat Transfer*, 3rd edn. (McGraw Hill, New York, 1998)
26. M. Wang, N. Pan, Mater. Sci. Eng. R **63**, 1 (2008)

27. O. Krischer, K. Kröll, *Die Wissenschaftlichen Grundlagen der Trocknungstechnik*, 2nd edn. (Springer, Berlin, 1963)
28. D.R. Lide (ed.), *CRC Handbook of Chemistry and Physics* (CRC Press, Boca Raton, FL, 2003)
29. R. Bergman, *Wood Handbook—Wood as an Engineering Material, General Technical Report FPL-GTR-190* (U.S. Department of Agriculture, Forest Service, Forest Products Laboratory, Madison, WI, 2010)
30. E.A. Guggenheim, *Application of Statistical Mechanics* (Clarendon Press, Oxford, 1966)